Supporting Information

Multimodal Imaging-Guided Nanoreactor for Cooperative Combination of Tumor Starvation and Multiple Mechanisms-Enhanced Mild Temperature Phototherapy

Jin Cao,[a] Bin Qiao,[a] Yuanli Luo,[a] Chongqing Cheng,[b] Anyu Yang,[a] Mengzhu Wang,[c] Xun Yuan,[d] Kui Fan,[e] Maoping Li,[b]* and Zhigang Wang,[a]*

Dr. J. Cao, Dr. B. Qiao, Mrs. Y. Luo, Dr. A. Yang, Prof. Z. Wang
Institute of Ultrasound Imaging, the Second Affiliated Hospital of Chongqing Medical University, Chongqing, 400010, China
E-mail: 303507@hospital.cqmu.edu.cn
Dr. C. Cheng, Dr. M. li
Department of Ultrasound, the First Affiliated Hospital of Chongqing Medical University, Chongqing, 400010, China
E-mail: limaoping@hospital.cqmu.edu.cn
Mrs. M. Wang
Department of Oncology, The Second Affiliated Hospital of Chongqing Medical University, Chongqing 400010, China
Mr. X. Yuan
Department of Ophthalmology, The Second Affiliated Hospital of Chongqing Medical University, Chongqing 400010, China
Mr. K. Fan
Department of Nephrology, The Second Affiliated Hospital of Chongqing Medical University, Chongqing 400010, China

Part A: Methods

The values of the maximum velocities (Vmax) and the Michaelis−Menten constant (Km) of GOx were calculated by the following Equations[1-3].

(1) Beer−Lamberts law: $A = kbc$

(2) Michaelis−Menten equation: $$V0 = \frac{Vmax\ S}{KM + S}$$

Following the equation (2), the linear section of the time-dependent absorbance was acquired, from which corresponding initial velocities over glucose concentration were obtained to evaluate the catalytic activity of GOx. Based on equation (1), the absorbance variation could be transformed to the initial velocities (v_0), which was then plotted on the matching glucose concentration and further fitted to the Michaelis-Menten equation to calculate the kinetic constant (equation 2).

Where A represents the absorbance value, k means the molar absorbance coefficient, b is the path length, and c is the molar concentration. v_0 means the initial velocity of the reaction, V_{max} represents the maximal velocity of reaction, S means the substrate concentration, and K_M represents the Michaelis–Menten constant. Therefore, the Km was calculated to be 61.40 mM, and the Vmax was calculated to be 1.168 × 10^{-6} M s^{-1} for GOx. While the Km and the Vmax were calculated to be 113.74 mM and 2.28 × 10^{-6} M s^{-1} for Fe-PDAP/GOx/ICG (Figure S8).

Calculation of $^1O_2$ quantum yield:

The singlet oxygen quantum yield (ΦΔ) was determined by using ICG as a reference (ΦΔ = 0.2%) and calculated by the following Equation[4, 5].

$$\Phi\Delta\ (sample) = \Phi\Delta\ (ICG)\frac{rsample\ /Asample}{rICG/\ AICG} \quad (3)$$

Where $\Phi\Delta_{(sample)}$ and $\Phi\Delta_{(ICG)}$ are the $^1O_2$ quantum yield of sample and ICG, respectively. r_{sample} and r_{ICG} are the photodecomposition rates of DPBF resulting from sample and ICG, respectively. A_{sample} and A_{ICG} are the corresponding absorbances of sample and ICG at 780 nm.

Herein, both A_{ICG} and $A_{Fe\text{-}PDAP/GOx/ICG}$ were 0.628, $r_{Fe\text{-}PDAP/GOx/ICG}$ was 0.0008223, and r_{ICG} was 0.0004174 (Figure S15)**.** Thus, the $^1O_2$ quantum yield of Fe-PDAP/GOx/ICG can be calculated to be ~0.39%.

Calculation of the Photothermal Conversion Efficiency:

The photothermal conversion efficiency (η) of Fe-PDAP/GOx/ICG was calculated following the method reported by Roper's team[6, 7]. Briefly, 100 μL of Fe-PDAP/GOx/ICG dispersion at a concentration of 12.5 μg/mL in a 96-well plate were irradiated by 808 nm laser at 1 W/cm^2, and then the laser was turned off when the temperature of the solutions increased to a steady-state. The whole process of dispersion's temperature change was recorded by an infrared thermal imaging camera (Fotric 226, Shanghai, China). The η was calculated based on the following formula：

$$\eta = \frac{hA\ \Delta T_{Max} - Qs}{I\ (1 - 10^{-A_\lambda})} \quad (4)$$

$$\tau_s = \frac{\sum_i m_i C_{p,i}}{hA} \quad (5)$$

From formula (4), η was regarded as conversion efficiency value, ΔT_{max} was regarded as the temperature change between the highest and lowest equilibrium temperature. Qs was related to the light absorbance of distilled water here, which was regarded as the heat energy produced by

the distilled water. I was regarded as the laser power density. A_λ was regarded as the absorbance of the dispersion at 808 nm according to the UV-Vis spectrum. The value of hA could be calculated from the formula (5).

From equation (5), the mass of water (m) and the heat capacity of water (C) were regarded as the mass of solution and its heat capacity, respectively. The time constant (τ_s) of the heating system was determined by applying the linear time-dependent data collected during the cooling period.

Herein, m was 200 mg, C was 4.2 J $g^{-1}K^{-1}$ and τ_s of Fe-PDAP/GOx/ICG was determined to be 146.3 s as shown in Figure S16a**.** According to equation (4), the hA was calculated to be 12.6×10^{-3} $W^{-1}K$.

η value of Fe-PDAP/GOx/ICG was subsequently calculated in detail. ΔT_{max} value was 25.3℃ as shown in Figure S16b**.** Qs here was measured to be 0.93357 mW. I was the laser power density that is 1 W/cm^2. A_λ was the absorbance of 100 μg/mL Fe-PDAP/GOx/ICG at 780 nm in the UV-Vis spectrum which was determined to be 2.739 According to equation (4), the *η* of Fe-PDAP/GOx/ICG was calculated to be 29.18%.

Combination index (CI) **is calculated by the following Equation:**

(6) $$CI = \frac{DA|A+B+C}{DA} + \frac{DB|A+B+c}{DB} + \frac{DC|A+B+c}{DC}$$

where $DA|A$+B+C, $DB|A$+B+C, and $DC|A$+B+C are the doses for PDT, PTT, and starvation therapy in combined therapy, respectively, which are the half-maximal inhibitory concentration (IC50). DA is the dose for PDT, DB is the dose for PTT and Dc is the dose for starvation therapy, which are IC50 for MDA-MB-231 cells. The CI value reflects the interaction effect of chemotherapy and

photothermal therapy. CI < 0.6 suggests strong synergism; 0.6 < CI < 0.8 indicates moderate synergism; 0.8 < CI < 0.9 indicates slight synergism; and 0.9 < CI < 1.1 indicates an additive effect[8, 9].

Part B: Supporting Figures

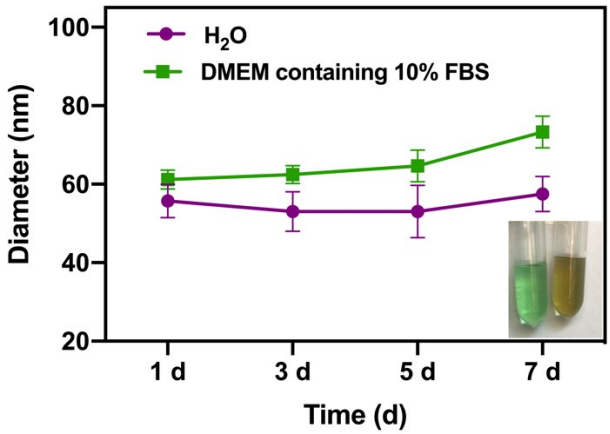

Figure S1. Size changes in 7 days observations in H_2O and DMEM containing 10% FBS. Inset: a corresponding photograph of Fe-PDAP/GOx/ICG in H_2O and DMEM containing 10% FBS. Results were expressed as mean ± SD. (*n* = 3).

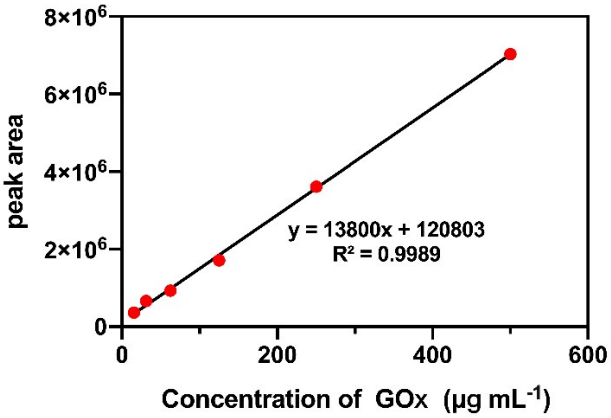

Figure S2. The standard curve of GOx and the equation of linear regression.

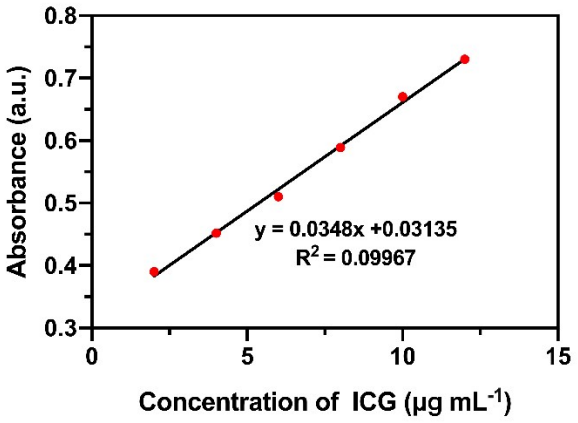

Figure S3. The calibration curve of ICG obtained from the absorbance at 780 nm with different concentration of ICG.

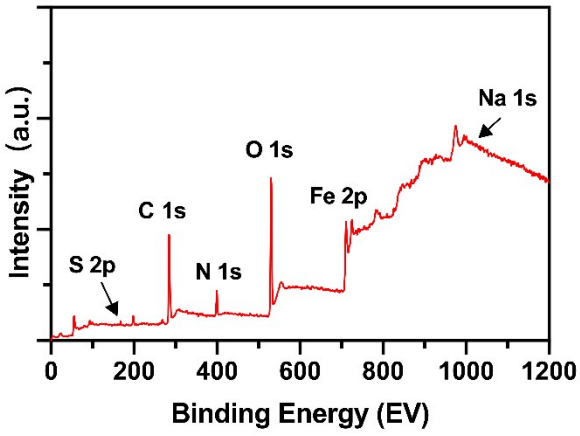

Figure S4. XPS survey spectrum of Fe-PDAP/GOx/ICG.

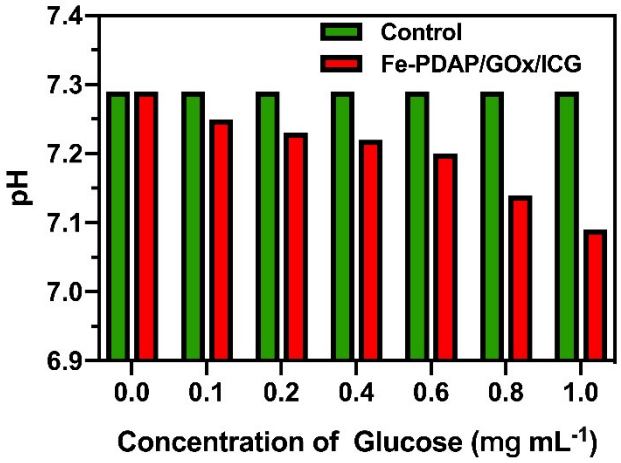

Figure S5. Glucose concentration-related pH changes after treatment with H_2O and Fe-PDAP/GOx/ICG for 1 h.

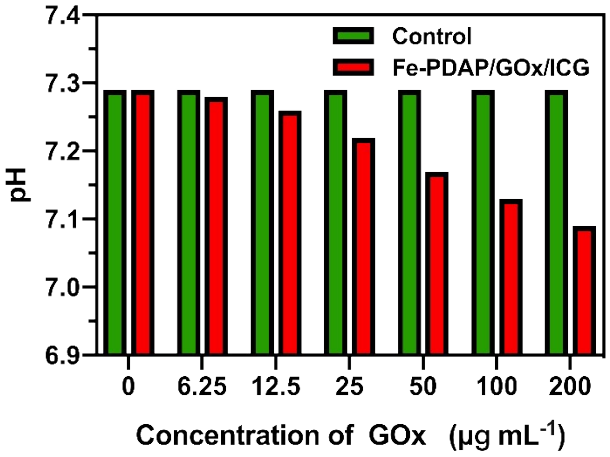

Figure S6. GOx concentration related pH changes after treatment with H_2O and Fe-PDAP/GOx/ICG for 1 h in the presence of 1 mg mL^{-1} glucose.

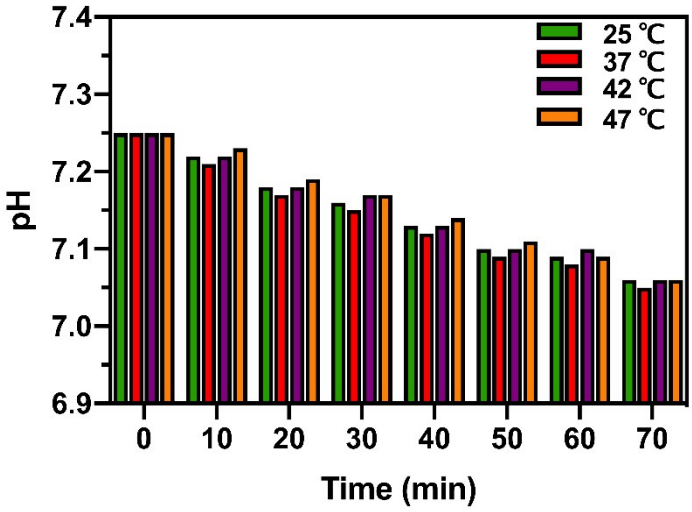

Figure S7. The pH changes of glucose solution added Fe/GOx/ICG under different temperatures.

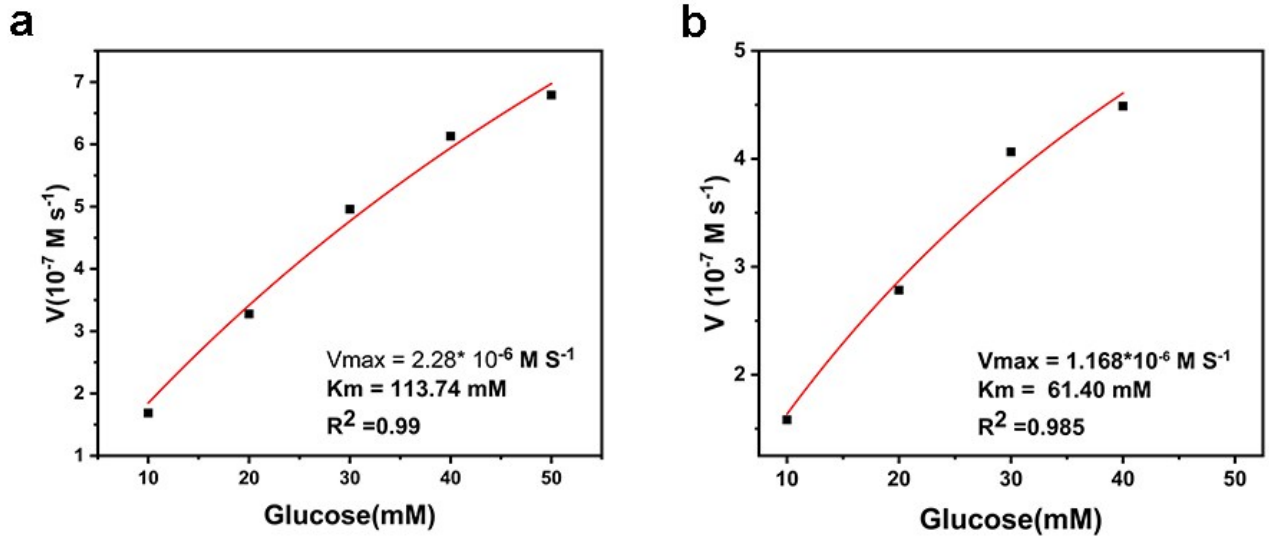

Figure S8. Michaelis–Menten kinetics of (a)Fe-PDAP/GOx/ICG and (b)GOx

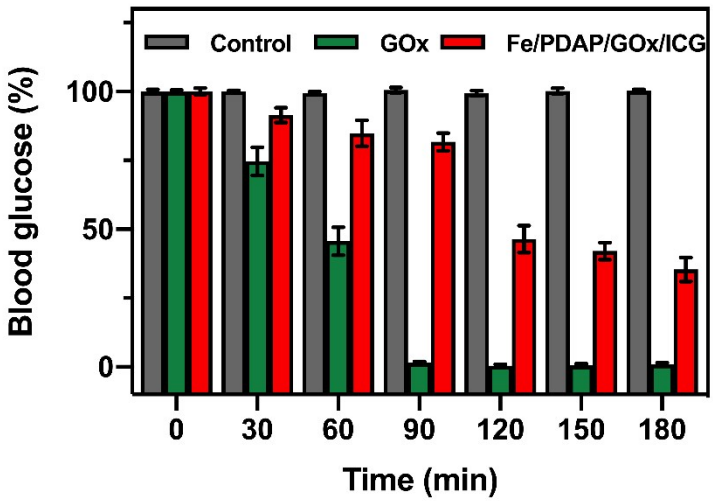

Figure S9: In vitro blood glucose level of FBS after treating with the solution of GOx or Fe-PDAP/GOx/ICG (The data was shown as mean ± SD, n=3 per group).

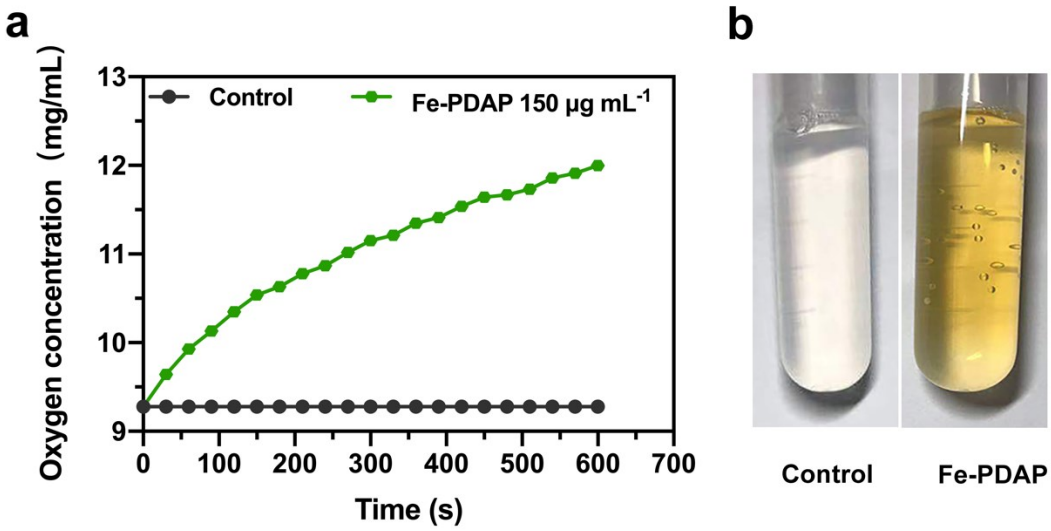

Figure S10. a) The O_2 concentration changes in the H_2O_2 solution after the addition of Fe-PDAP. b) The macroscopic images of the solutions in the presence of H_2O_2.

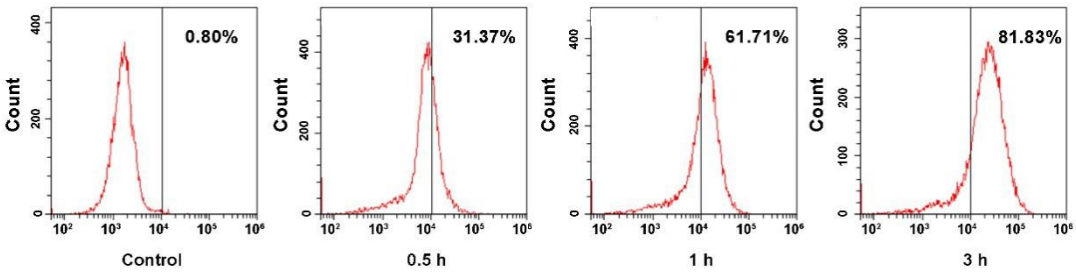

Figure S11. Intracellular uptake results of DiI labeled Fe-PDAP/GOx/ICG determined by flow cytometry.

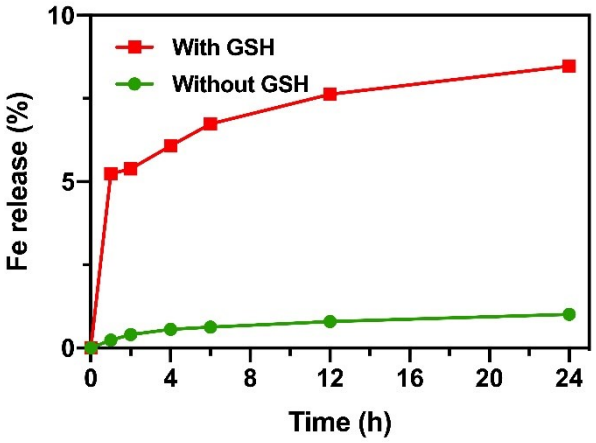

Figure S12. Fe release profiles of Fe-PDAP/GOx/ICG with or without GSH treatment.

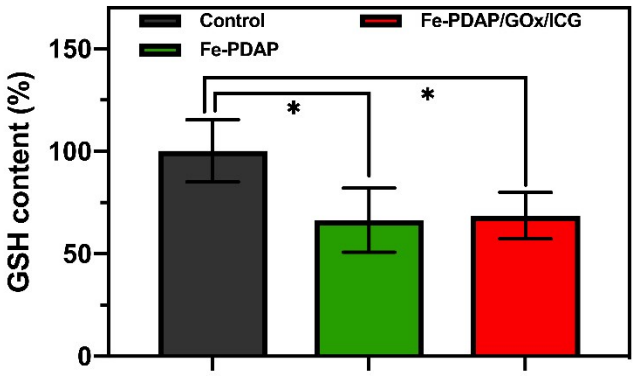

Figure S13. The content of GSH after treatment with Fe-PDAP and Fe-PDAP/GOx/ICG. (The data was shown as mean ± SD, n=3 per group, *P < 0.05).

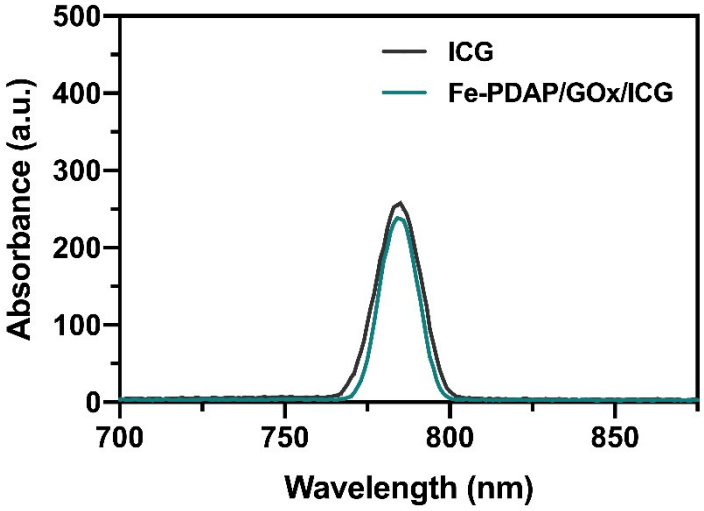

Figure S14. The fluorescence spectrum of Fe-PDAP/GOx/ICG and ICG.

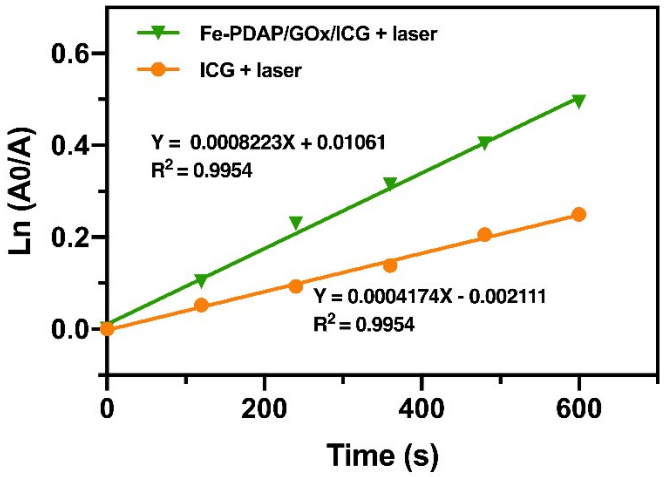

Figure S15. Rate constants for DPBF decomposition in the presence of ICG and Fe-PDAP/GOx/ICG after laser irradiation.

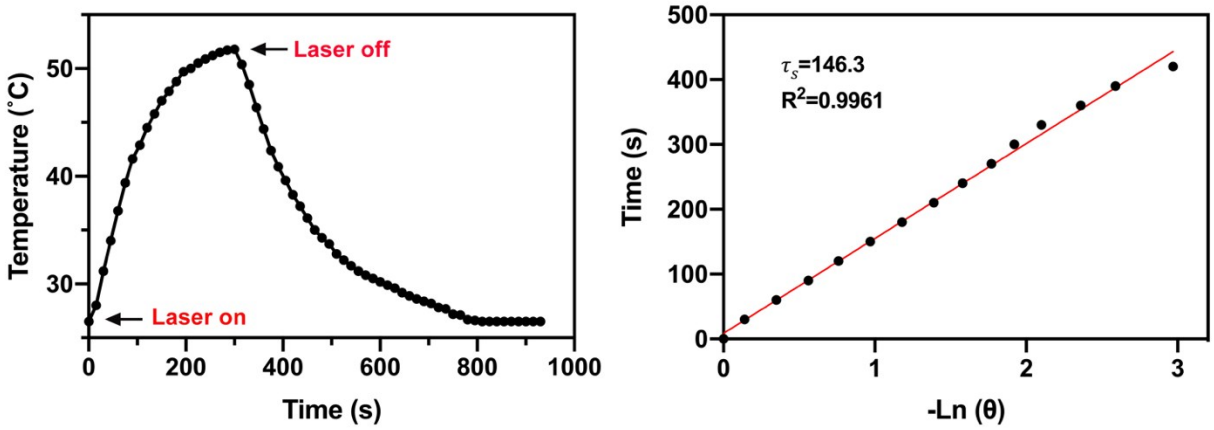

Figure S16. a) The photothermal response of Fe-PDAP/GOx/ICG aqueous dispersion (12.5 μg mL^{-1}) under NIR irradiation (808 nm, 1 W cm^{-2}). The laser was shut off until once the temperature reached a steady-state value. b) The time constant for heat transfer calculated from the cooling period of Figure S14a.

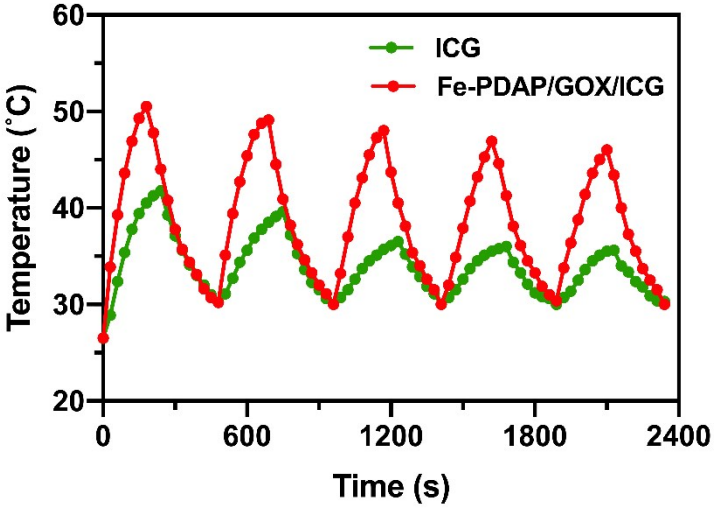

Figure S17. Heating curves of ICG and Fe-PDAP/GOx/ICG suspension for five cycles.

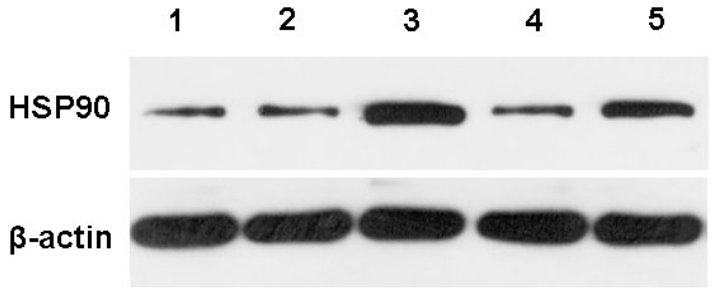

Figure S18. Western blotting analysis of HSP 90 expression in MDA-MB-231 cells with different treatments (1: control; 2: Fe-PDAP/ICG only; 3: Fe-PDAP/ICG with NIR irradiation; 4: Fe-PDAP/GOx/ICG only; 5: Fe-PDAP/GOx/ICG with NIR irradiation.)

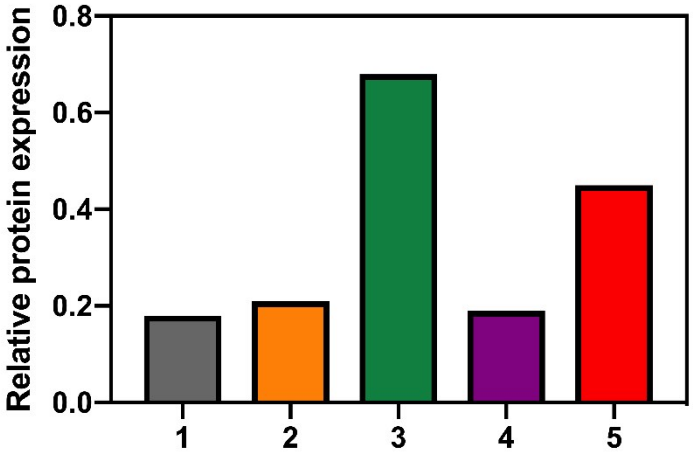

Figure S19. The corresponding quantitative results of HSP90 expression.

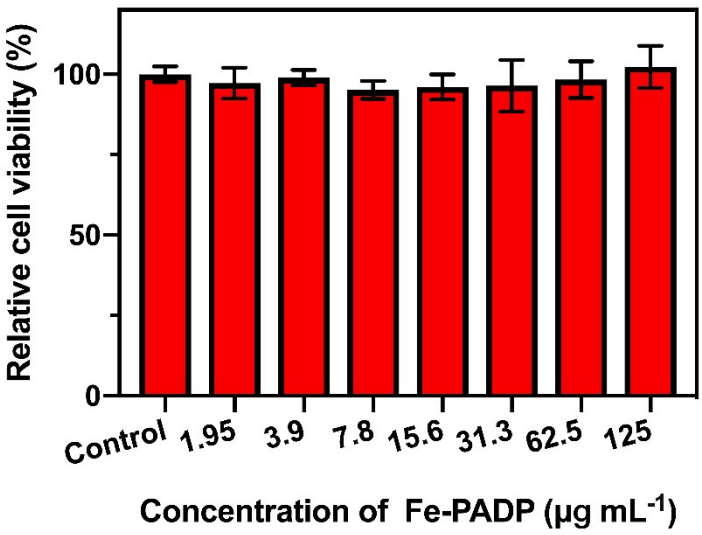

Figure S20. In vitro cytotoxicity profiles of Fe-PDAP. (The data was shown as mean ± SD, n=3 per group)

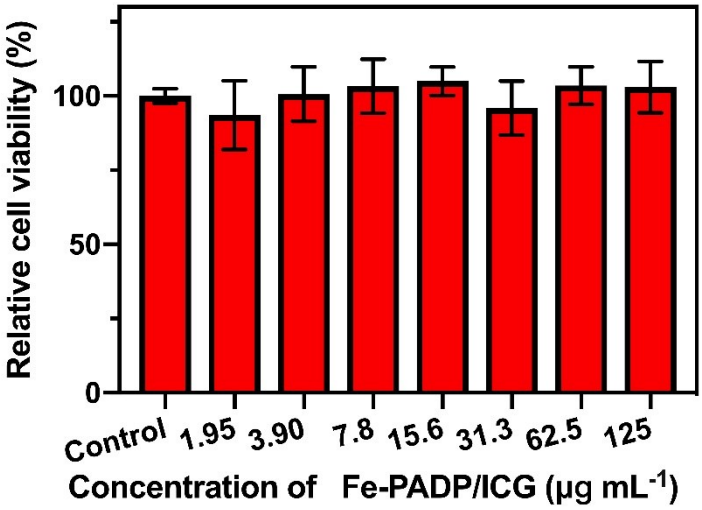

Figure S21. In vitro cytotoxicity profiles of Fe-PDAP. (The data was shown as mean ± SD, n=3 per group).

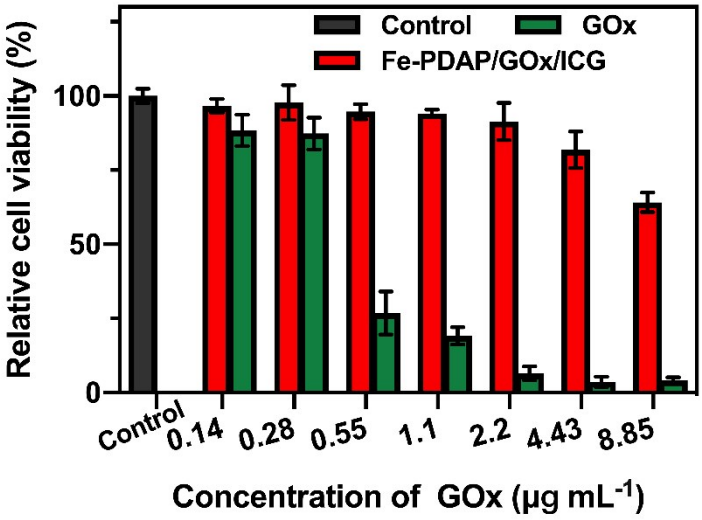

Figure S22. Cytotoxicity assay of Fe-PDAP/GOx/ICG and GOx incubated with MDA-MB-231 cells. (The data was shown as mean ± SD, n=3 per group).

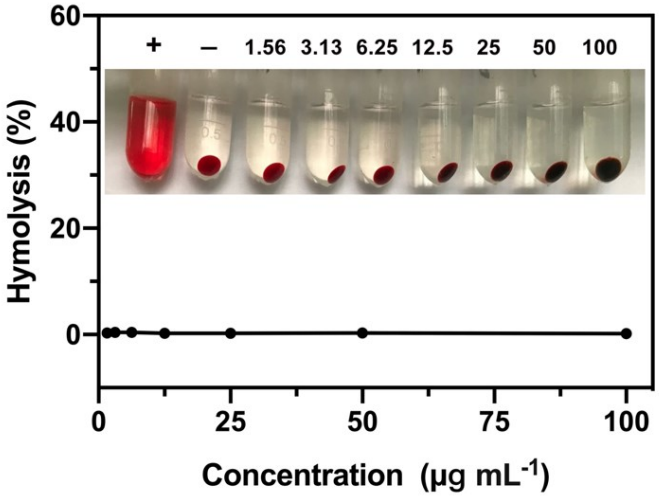

Figure S23. Hemolysis of Fe-PDAP/GOx/ICG after incubation with red blood cells (RBC) at various concentrations (right seven tubes) for 2 h. The RBC dispersed in PBS was set as a negative control, while dispersed in deionized water was set as a positive control (left two tubes). Inset: hemolysis photographs after centrifugation.

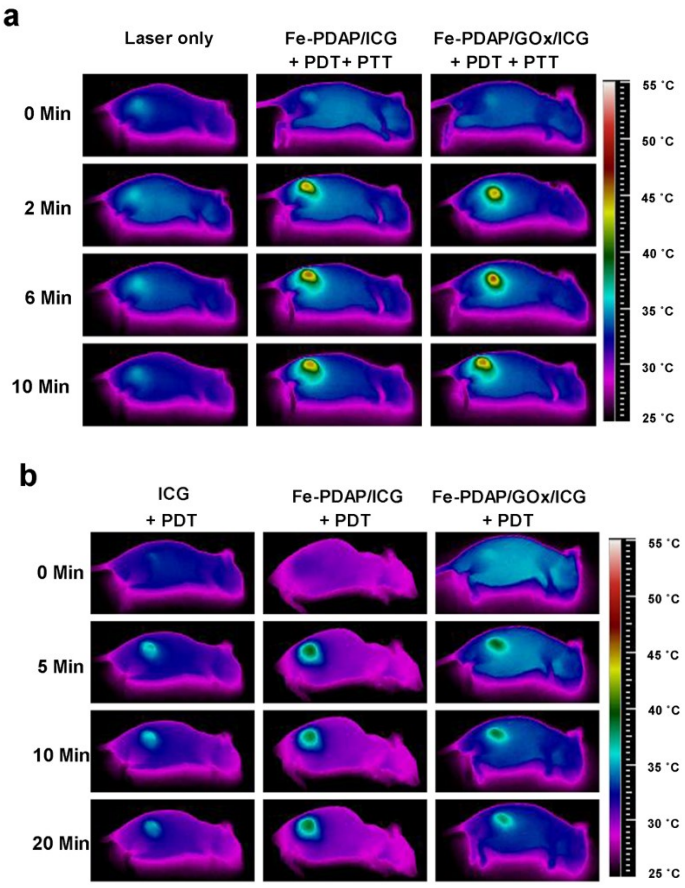

Figure S24. (a) Thermal images of MDA-MB-231-tumor-bearing mice from different treating groups under 808m laser irradiation (1 W cm^{-2}, 10 min). (b) Thermal images of MDA-MB-231-tumor-bearing mice from different treating groups plus interval laser irradiation (30 seconds irradiation followed by 30 seconds interval, 1 W cm^{-2} for 20 cycles).

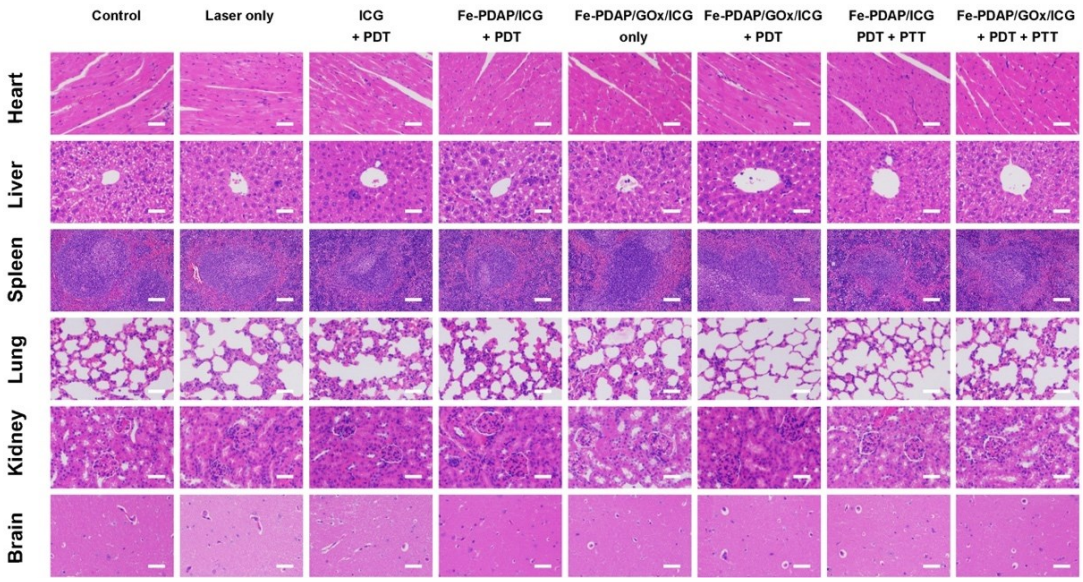

Figure S25. H&E staining of the major organs (heart, liver, spleen, lungs, and kidneys) of MDA-MB-231 tumor-bearing mice after different treatments. All the scale bars are 50 μm.

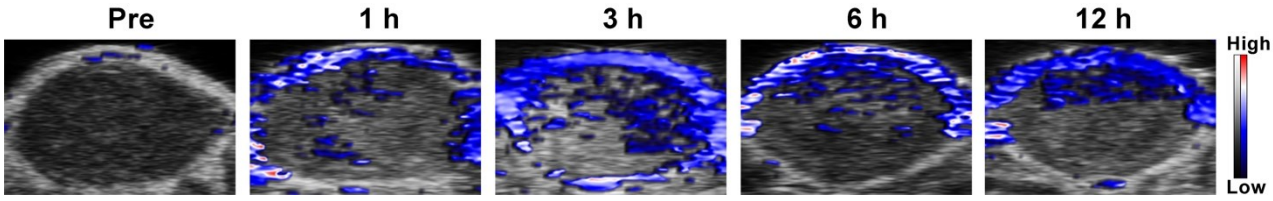

Figure S26. In vivo oxyhemoglobin saturation of MDA-MB-231 tumor after intravenous injection of Fe-PDAP/GOx/ICG at different time points.

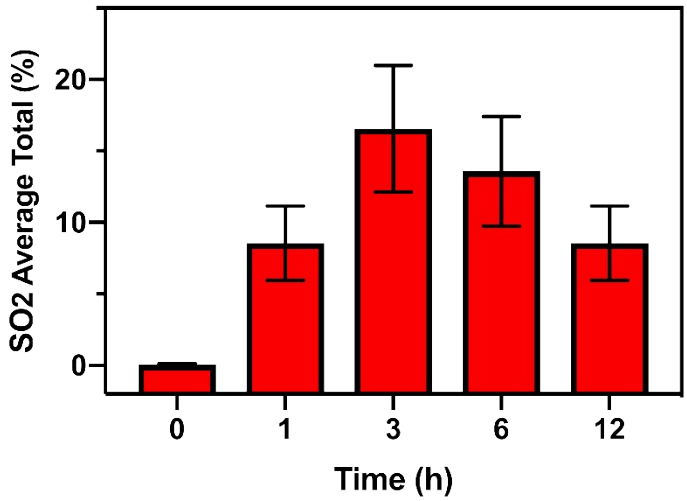

Figure S27. Quantification of oxyhemoglobin saturation at tumor sites by measuring the ratios of oxygenated hemoglobin (λ = 850 nm) and deoxygenated hemoglobin (λ = 750 nm). (Values are means ± SD, n = 3)

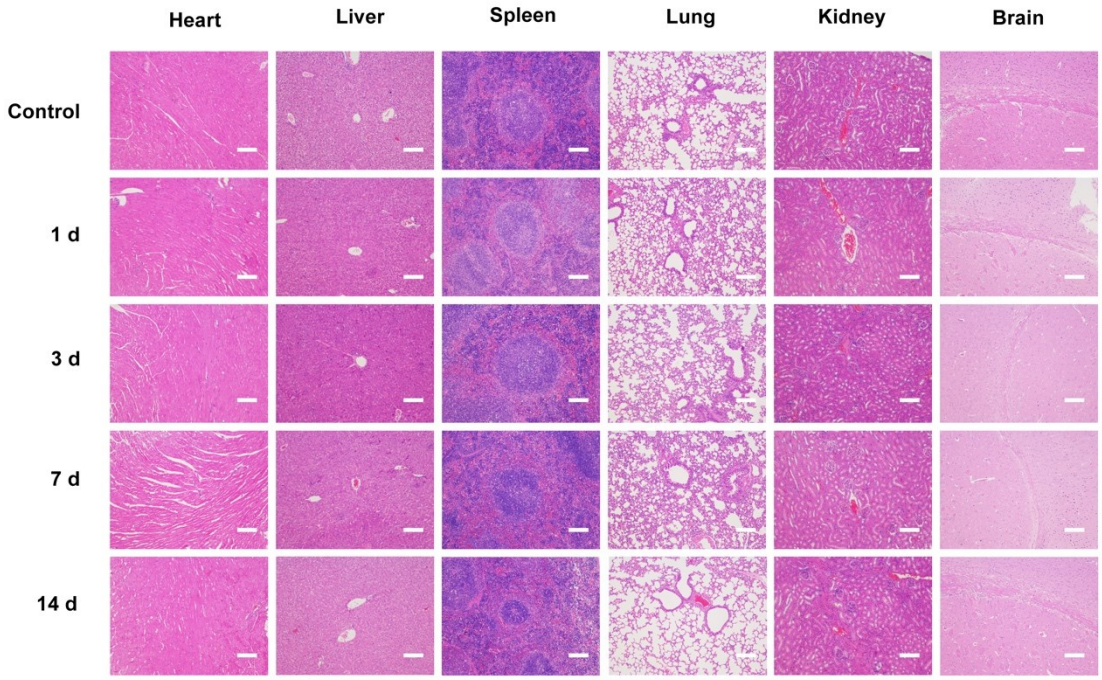

Figure S28. H&E staining of major organs from the control group and experimental groups 1, 3, 7, and 14 d post intravenous injection of Fe-PDAP/GOx/ICG. All the scale bars are 200 μm.

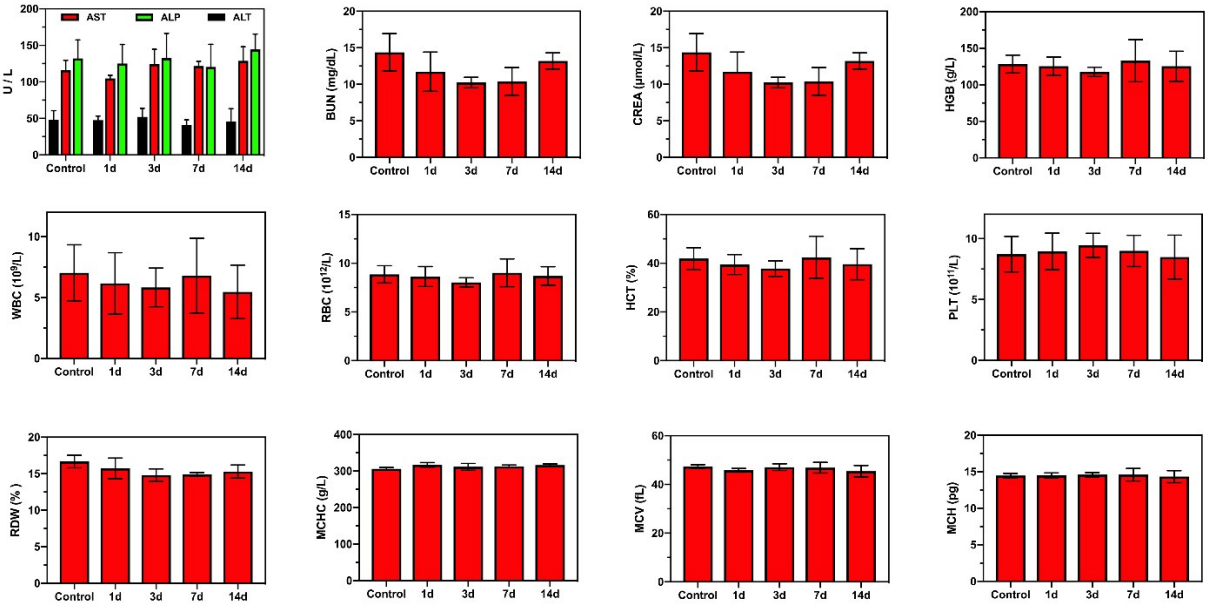

Figure S29. Blood biochemical examination of mice from the control group and the experiment groups 1, 3, 7, and 14 d after intravenous injection of Fe-PDAP/GOx/ICG. (The data was shown as mean ± SD, n=3 per group).

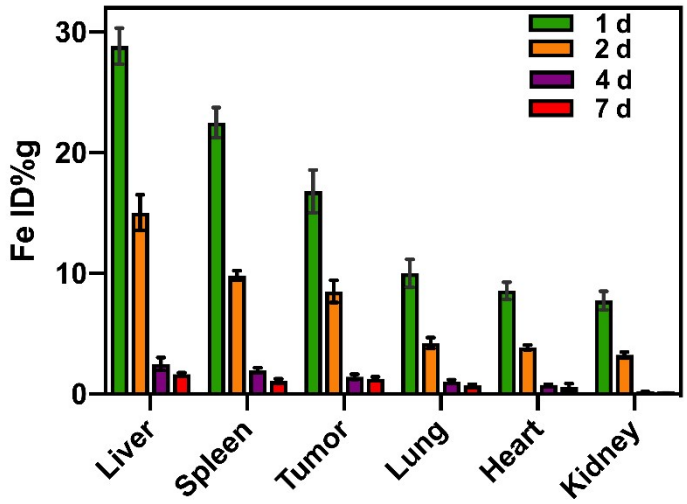

Figure S30. The biodistribution of Fe (% injected dose (ID) of Fe per gram of tissues) in main tissues and tumors at 1, 2, 4, and 7 d after intravenous administration of Fe-PDAP/GOx/ICG nanoreactor.

REFERENCES:

1. R. Liang, Y. Li, M. Huo, H. Lin and Y. Chen, *ACS Applied Materials & Interfaces*, 2019, **11**, 42917-42931.
2. W. Feng, X. Han, R. Wang, X. Gao, P. Hu, W. Yue, Y. Chen and J. Shi, *Adv Mater*, 2019, **31**, e1805919.
3. S. Gao, H. Lin, H. Zhang, H. Yao, Y. Chen and J. Shi, *Adv Sci (Weinh)*, 2019, **6**, 1801733.
4. S. Wang, L. Shang, L. Li, Y. Yu, C. Chi, K. Wang, J. Zhang, R. Shi, H. Shen, G. I. Waterhouse, S. Liu, J. Tian, T. Zhang and H. Liu, *Adv Mater*, 2016, **28**, 8379-8387.
5. Q. Wang, J. Xu, R. Geng, J. Cai, J. Li, C. Xie, W. Tang, Q. Shen, W. Huang and Q. Fan, *Biomaterials*, 2020, **231**, 119671.
6. Y. Liu, K. Ai, J. Liu, M. Deng, Y. He and L. Lu, *Advanced Materials*, 2013, **25**, 1353-1359.
7. T. Liu, M. Zhang, W. Liu, X. Zeng, X. Song, X. Yang, X. Zhang and J. Feng, *ACS Nano*, 2018, **12**, 3917-3927.
8. L. Cheng, F. Zhang, S. Wang, X. Pan, S. Han, S. Liu, J. Ma, H. Wang, H. Shen, H. Liu and Q. Yuan, *Angewandte Chemie International Edition*, 2019, **58**, 7728-7732.
9. S. Barua and S. Mitragotri, *ACS Nano*, 2013, **7**, 9558-9570.